flashes during the asymptotic giant branch phase of stellar evolution (AGB stars); such stars have been identified as the site of the main component of s-process nucleosynthesis[23]. According to estimates given in refs 2 and 24, the consequence of our modified rate is up to a factor of 3 less carbon produced in AGB stars.

Finally, as the first stars in the Universe lacked the heavy elements catalysing hydrogen burning, the evolution of these stars is believed to be very sensitive to the triple-α reaction at temperatures below 10^8 K. For these primordial stars with masses similar to that of the Sun, a small amount of ^{12}C is produced by the triple-α process during the phase of central hydrogen burning. When the ^{12}C abundance reaches a critical level the CNO cycle is ignited[4]; this level may be reached in half the time with our higher rate at the lowest temperatures. This is important for the subsequent evolution of the star, and for how the ashes of the nuclear burning, the basis for the next generation of stars, are transported to the outer layers of the star and ejected into the interstellar medium. Stellar model calculations testing this effect using our triple-α rate are in progress (J. Christensen-Dalsgaard, personal communication). □

Methods

The ISOL method

The ^{12}N activity (half-life 11.0 ms) was produced at the IGISOL facility[25] of the Jyväskylä Accelerator Laboratory in Finland by using the ^{12}C(p,n)^{12}N reaction with a 40-MeV proton beam. The ^{12}B activity (half-life 20.20 ms) came from *in situ* decay of ^{12}Be (half-life 21.5 ms) produced by 1-GeV proton-induced spallation reactions on a thick Ta target at the ISOLDE facility[26], CERN. In both experiments, the produced nuclei were extracted, accelerated to 40 keV, mass separated and finally transferred to a detection area where they were stopped in a thin carbon collection foil. This is known as the isotope separation on-line (ISOL) method.

By studying the β-decays of both ^{12}B and ^{12}N we reduce sensitivity for systematic errors. These two nuclei release significantly different energies in their β-decays (known as the Q_β energy), which causes different excitation energies in ^{12}C to be populated with different weights owing to the strong energy dependence of the β-neutrino phase-space. The product of this phase-space factor and the partial half-life of a transition is the ft-value, which is inversely proportional to the nuclear matrix element.

Detection system

The detection system consisted of two double sided silicon strip detectors (DSSSDs) placed on either side of the collection foil. Owing to the presence of very low energy α-particles in these decays, attention to energy loss effects in the collection foil and detector dead-layers is crucial. In the ^{12}N experiment, standard DSSSDs were used and a special calibration and analysis procedure applied[27], whereas in the ^{12}B experiment a new DSSSD design with reduced dead-layers was used[28]. Significantly reduced energy detection thresholds were achieved in the ^{12}B experiment, as may be seen in Fig. 2 where the ^{12}B spectrum extends well below that from ^{12}N. The efficiency for detecting two or three α-particles is determined from Monte Carlo simulations separately for the two experiments.

R-matrix fits

These are commonly used in atomic, nuclear and particle physics to achieve a phenomenological understanding of data[14]. We apply a formalism developed specifically for β-decay[29]. The method is used in general to connect observed peak structures with parameter values of the states involved, in particular when interference effects or threshold effects are dominant. In such cases, the position of states does not always coincide with maxima of peaks in the observed spectra. The parameter values quoted here are the so-called observed R-matrix parameters, which are introduced to correct for this discrepancy. Here we use the same parameters for the Hoyle resonance as NACRE: resonance energy 0.3798 MeV, α-width 8.3 eV and γ-width 3.7 meV. The interference effect is seen in Fig. 2 as an enhancement of the low-energy region between the two resonances and a decrease on the high-energy side of the broad resonance. It causes the shift of the energy of the broad 0^+ resonance from the previous value near 10 MeV to 11.23(5) MeV even when using observed R-matrix parameters.

Received 7 September; accepted 24 November 2004; doi:10.1038/nature03219.

1. Wallerstein, G. *et al.* Synthesis of the elements in stars: 40 years of progress. *Rev. Mod. Phys.* **69,** 995–1084 (1997).
2. Austin, S. in *Proc. 8th Nuclei in the Cosmos Conf., Nucl. Phys. A* (in the press).
3. Angulo, C. *et al.* A compilation of charged-particle induced thermonuclear reaction rates. *Nucl. Phys. A* **656,** 3–183 (1999).
4. Siess, L., Livio, M. & Lattanzio, J. Structure, evolution, and nucleosynthesis of primordial stars. *Astrophys. J.* **570,** 329–343 (2002).
5. Fröhlich, C. *et al.* Composition of the innermost supernova ejecta. *Astrophys. J.* (submitted).
6. Pruet, J., Woosley, S. E., Buras, R., Janka, H.-T. & Hofmann, R. D. Nucleosynthesis in the hot convective bubble in core-collapse supernovae. *Astrophys. J.* (submitted).
7. Ajzenberg-Selove, F. Energy levels of light nuclei A=11–12. *Nucl. Phys. A* **506,** 1–158 (1990).
8. Hoyle, F., Dunbar, D. N. F., Wenzel, W. A. & Whaling, W. A state in ^{12}C predicted from astrophysical evidence. *Phys. Rev.* **92,** 1095 (1953).
9. Dunbar, D. N. F., Pixley, R. E., Wenzel, W. A. & Whaling, W. The 7.68 MeV state in ^{12}C. *Phys. Rev.* **92,** 649–650 (1953).
10. Cook, C. W., Fowler, W. A., Lauritsen, C. C. & Lauritsen, T. B^{12}, C^{12}, and the red giants. *Phys. Rev.* **107,** 508–515 (1957).
11. Morinaga, H. Interpretation of some of the excited states of 4n self-conjugate nuclei. *Phys. Rev.* **101,** 254–258 (1956).
12. Cook, C. W., Fowler, W. A., Lauritsen, C. C. & Lauritsen, T. High energy alpha particles from B^{12}. *Phys. Rev.* **111,** 567–571 (1958).
13. Fynbo, H. O. U. *et al.* Clarification of the three-body decay of ^{12}C(12.71 MeV). *Phys. Rev. Lett.* **91,** 082502 (2003).
14. Lane, A. M. & Thomas, R. G. R-matrix theory of nuclear reactions. *Rev. Mod. Phys.* **30,** 257–353 (1958).
15. John, B., Tokimoto, Y., Lui, Y.-W., Clark, H. L., Chen, X. & Youngblood, D. H. Isoscalar electric multipole strength in ^{12}C. *Phys. Rev. C* **68,** 014305 (2003).
16. Itoh, M. *et al.* Study of the cluster state at $E_x = 10.3$ MeV in ^{12}C. *Nucl. Phys. A* **738,** 268–272 (2004).
17. Fowler, W. A. Experimental and theoretical nuclear astrophysics: The quest for the origin of the elements. *Rev. Mod. Phys.* **56,** 149–179 (1984).
18. Weaver, T. A. & Woosley, S. E. Nucleosynthesis in massive stars and the ^{12}C(α,γ)^{16}O reaction rate. *Phys. Rep.* **227,** 65–96 (1993).
19. Schlattl, H., Heger, A., Oberhummer, H., Rauscher, T. & Csótó, A. Sensitivity of the C and O production on the 3α rate. *Astrophys. Space Sci.* **291,** 27–56 (2004).
20. Delano, M. D. & Cameron, A. G. W. Nucleosynthesis in neutron rich supernova ejecta. *Astrophys. Space Sci.* **10,** 203–226 (1971).
21. Schatz, H. *et al.* Rp-process nucleosynthesis at extreme temperature and density conditions. *Phys. Rep.* **294,** 167–263 (1998).
22. Woosley, S. E. *et al.* Models for Type I X-ray bursts with improved nuclear physics. *Astrophys. J. Supp.* **151,** 75–102 (2004).
23. Käppeler, F., Thielemann, F.-K. & Wiescher, M. Current quests in nuclear astrophysics and experimental approaches. *Annu. Rev. Part. Sci.* **48,** 175–251 (1998).
24. Herwig, F. & Austin, S. M. Nuclear reaction rates and carbon star formation. *Astrophys. J.* **613,** L73–L76 (2004).
25. Äystö, J. Development and applications of the IGISOL technique. *Nucl. Phys. A* **693,** 477–494 (2001).
26. Kugler, E. The ISOLDE facility. *Hyperfine Interact.* **129,** 23–42 (2000).
27. Bergmann, U. C., Fynbo, H. O. U. & Tengblad, O. Use of Si strip detectors for low-energy particles in compact geometry. *Nucl. Instrum. Methods A* **515,** 657–664 (2003).
28. Tengblad, O., Bergmann, U. C., Fraile, L. M., Fynbo, H. O. U. & Walsh, S. Novel thin window design for a large-area silicon strip detector. *Nucl. Instrum. Methods A* **525,** 458–464 (2004).
29. Barker, F. C. & Warburton, E. K. The beta-decay of ^{8}He. *Nucl. Phys. A* **487,** 269–278 (1988).
30. Schwalm, D. & Povh, B. Alpha particles following the β-decay of ^{12}B and ^{12}N. *Nucl. Phys.* **89,** 401–411 (1966).

Acknowledgements This research was supported by the Academy of Finland under the Finnish Centre of Excellence Programme, by the Spanish Agency CICYT, and by the European Union Fifth Framework Programme 'Improving Human Potential—Access to Research Infrastructure'. Discussions with J. Christensen-Dalsgaard and C. Fröhlich are acknowledged.

Competing interests statement The authors declare that they have no competing financial interests.

Correspondence and requests for materials should be addressed to H.F. (fynbo@phys.au.dk).

Systematic design of chemical oscillators using complexation and precipitation equilibria

Krisztina Kurin-Csörgei[1], Irving R. Epstein[2] & Miklós Orbán[1]

[1]*Department of Inorganic and Analytical Chemistry, L. Eötvös University, H-1518 Budapest 112, PO Box 32, Hungary*
[2]*Department of Chemistry and Volen Center for Complex Systems, MS 015, Brandeis University, Waltham, Massachusetts 02454-9110, USA*

Concentration oscillations are ubiquitous in living systems, where they involve a wide range of chemical species. In contrast, early *in vitro* chemical oscillators were all derived from two accidentally discovered reactions[1–3] based on oxyhalogen chemistry. Over the past 25 years, the use of a systematic design algorithm[4,5], in which a slow feedback reaction periodically drives a bistable system in a flow reactor between its two steady states, has increased the list of oscillating chemical reactions to dozens of systems. But these oscillating reactions are still con-

fined to a handful of elements that possess multiple stable oxidation states: halogens, sulphur and some transition metals[6]. Here we show that linking a 'core' oscillator to a complexation or precipitation equilibrium can induce concentration oscillations in a species participating in the equilibrium. We use this method to design systems that produce periodic pulses of calcium, aluminium or fluoride ions. The ability to generate oscillations in elements possessing only a single stable oxidation state (for example, Na^+, F^-, Ca^{2+}) may lead to reactions that are useful for coupling to or probing living systems, or that help us to understand new mechanisms by which periodic behaviour may arise.

The approach we take starts from the observation[7] that many chemical oscillators occur in 'families', which have in common a 'minimal' or 'core' set of reactions, that is, a 'primary oscillophor'[8], which produces the essential oscillatory dynamics. To bring about periodic behaviour in a chosen species S, rather than trying to build an oscillatory reaction directly around the chemistry of S, we seek instead to solve two simpler subproblems. We first try to identify a fast equilibrium (reaction E) in which S participates, and then attempt to find a 'core' oscillatory reaction (reaction O) that periodically produces and consumes a species C that shifts the position of that equilibrium. If O has a large and rapid effect on E, while E has little or no effect on the behaviour of O, then we can expect [S] to oscillate with a frequency close to that of the unperturbed reaction O. The concept is illustrated schematically in Fig. 1.

To make this scheme more concrete, we take S to be Ca^{2+} and E to be the formation of the CaEDTA (EDTA = ethylenediaminetetraacetic acid) complex:

$$Ca^{2+} + EDTA^{2-} \leftrightarrow CaEDTA$$
$$K_f = [CaEDTA]/[Ca^{2+}][EDTA^{2-}] = 4.9 \times 10^{10} \quad (1)$$

This equilibrium, which has formation constant K_f above pH 12, where the EDTA is completely deprotonated, displays a strong dependence on $[H^+]$ at lower pH (ref. 9), with conditional (pH-dependent) formation constant $K'_f = 1.27$ at pH 3.00, and $K'_f = 1.13 \times 10^6$ at pH 6.00, resulting in the fraction of free Ca^{2+} changing from >99% to <1% as the pH rises from 3 to 6, thereby changing the state of protonation of the EDTA. For the 'core' reaction O, then, we seek a pH oscillator (in which species C is H^+) that oscillates within this range and whose components do not react significantly with either calcium or EDTA. The reaction of bromate, sulphite and ferrocyanide[10] (BrO_3^-–SO_3^{2-}–$Fe(CN)_6^{4-}$) in a continuous flow stirred tank reactor (CSTR), which oscillates between pH 2.7 and 6.5, meets these criteria.

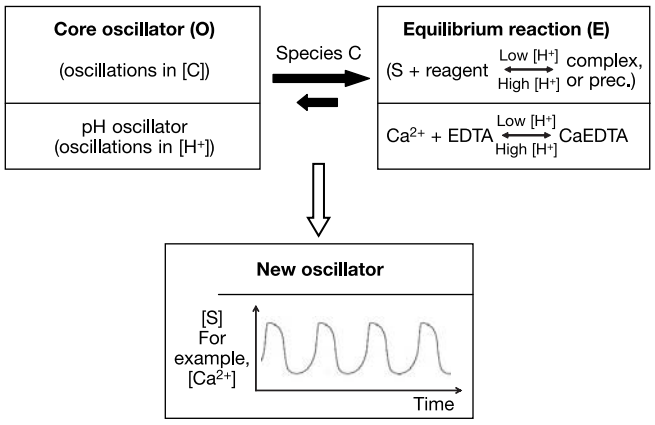

Figure 1 Schematic diagram of the basic elements for oscillator design. The core reaction O on the left generates oscillations in species C, which affects the equilibrium reaction E on the right, producing oscillations in the desired species S in the 'new oscillator' below the open arrow. Solid arrows indicate that reaction O has a much stronger effect on reaction E than vice versa. Examples of reactions are given in the lower part of each box.

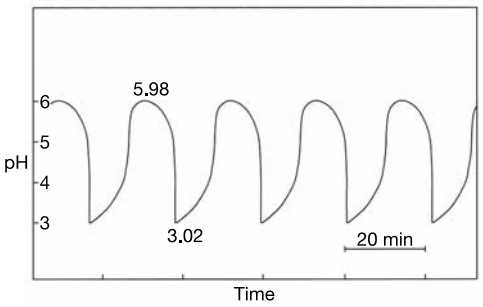

Figure 2 Oscillations of pH in the core BrO_3^-–SO_3^{2-}–$Fe(CN)_6^{4-}$ oscillator. The reaction is carried out in the presence of 2.5×10^{-3} M EDTA in a CSTR of volume 40.0 cm^3 at 30 °C, the optimum temperature for reaction O to proceed in an oscillatory fashion. The reagents are introduced through four input tubes attached to a peristaltic pump (Gilson Minipuls 2). The excess reaction mixture is removed through a hole in the reactor cap by a second pump. Concentrations in the core oscillator: $[NaBrO_3] = 6.5 \times 10^{-2}$ M, $[Na_2SO_3] = 7.5 \times 10^{-2}$ M, $[K_4Fe(CN)_6] = 2 \times 10^{-2}$ M, $[H_2SO_4] = 1 \times 10^{-2}$ M. All chemicals are of analytical grade (Aldrich and Fisher) and are used without further purification. Flow rate (reciprocal residence time in the reactor) $k_0 = 1.45 \times 10^{-3}\ s^{-1}$. pH is measured with a combined glass (ThermoOrion) electrode.

Figure 2 shows the pH oscillations measured in the core BrO_3^-–SO_3^{2-}–$Fe(CN)_6^{4-}$ system under CSTR conditions. EDTA, as the disodium salt, was also present in order to assess its buffering effect on reaction O. When the input EDTA is replaced with CaEDTA, the pH oscillations induce a relatively large (about two orders of magnitude) change in the concentration of free Ca^{2+}. At high pH, the calcium is covalently bound as the CaEDTA complex. At low pH, the complex dissociates, and nearly all calcium is present as free Ca^{2+}. Consequently, both calcium ions and the ligand EDTA appear in pulses during the oscillatory pH cycles. The concentration of free Ca^{2+} can conveniently be monitored with a Ca^{2+}-ion selective electrode (ISE), which responds negligibly to the changes in concentration of the other species in the complete system. A typical recording is presented in Fig. 3. The oscillations in free $[Ca^{2+}]$ can be visualized by introducing arsenazo (III) dye. The colour of the reaction mixture alternates between cherry red (free dye) and violet (Ca-arsenazo complex).

The coupling of pH oscillators to pH-dependent complexation equilibria offers a particularly promising route to the construction of new oscillatory reactions, but we can imagine other approaches as well. Besides complexation equilibria, formation of a precipitate can

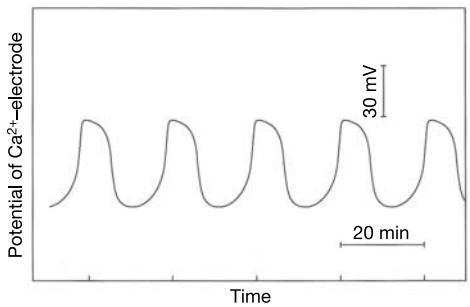

Figure 3 Oscillatory pulses of free Ca^{2+}. Potential (proportional to the logarithm of the free $[Ca^{2+}]$) is measured with a combined calcium-ISE (ThermoOrion) in the system of Fig. 2 with the input EDTA replaced by 2.5×10^{-3} M CaEDTA.

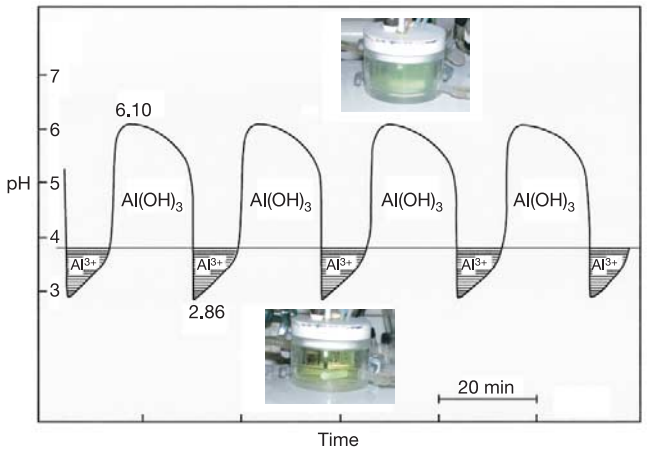

Figure 4 Periodic changes in the concentration of free Al^{3+}. The core BrO_3^-–SO_3^{2-}–$Fe(CN)_6^{4-}$ oscillator is augmented with a flow of $[Al(NO_3)_3] = 2.5 \times 10^{-3}$ M. The pulses of free $[Al^{3+}]$ (shaded areas in the graph showing pH measured while $Al^{3+}/Al(OH)_3$ is simultaneously followed visually) appear every 25 min and are maintained for about 8 min per pulse. The calculated change in free $[Al^{3+}]$ during a period is about five orders of magnitude. Insets show photos of the reactor when the reaction mixture is at low (clear solution) and high (turbid solution) pHs.

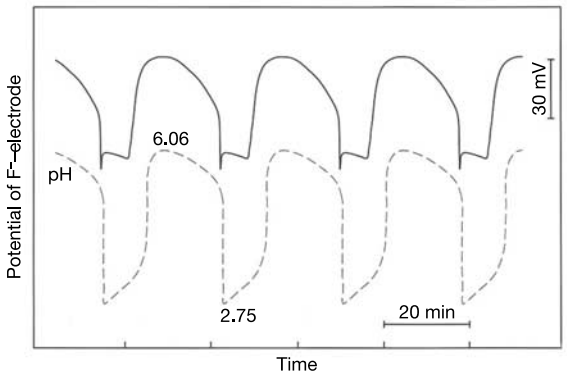

Figure 5 Oscillations in $[F^-]$. The BrO_3^-–SO_3^{2-}–$Fe(CN)_6^{4-}$ oscillator is augmented with flows of $[Al(NO_3)_3] = 2.5 \times 10^{-3}$ M and $[NaF] = 5 \times 10^{-3}$ M. $[F^-]$, measured as the potential (solid line) of a fluoride-ISE (Radelkis), oscillates between 8×10^{-5} and 3×10^{-3} M. Also shown are simultaneously monitored oscillations in pH (dashed line).

also be coupled to the core pH oscillator. We construct an Al^{3+} oscillator by choosing for equilibrium E the reaction:

$$Al(OH)_3(s) \leftrightarrow Al^{3+}(aq) + 3OH^-(aq)$$
$$K_{sp} = [Al^{3+}][OH^-]^3 = 1.3 \times 10^{-33} \quad (2)$$

where K_{sp} is the solubility product of the precipitate $Al(OH)_3$. Over the pH range 3–6, Al^{3+} goes from being extremely soluble ($1.33\ mol\ dm^{-3}$) to nearly totally insoluble ($1.33 \times 10^{-9}\ mol\ dm^{-3}$). Again, the BrO_3^-–SO_3^{2-}–$Fe(CN)_6^{4-}$ system proves suitable for coupling, and oscillations can be seen in the turbidity of the system as aluminium hydroxide periodically precipitates and redissolves. The results are shown in Fig. 4. The oscillations in pH are barely affected by the introduction of $Al(NO_3)_3$. As the pH passes through the critical value of 3.8, the reaction mixture becomes cloudy from formation of $Al(OH)_3$ or turns crystal clear, depending on the direction of the change in pH.

Although cationic oscillators are the most straightforward to design in this manner, we can construct pulses of anions as well. Fluoride oscillations, for example, can be generated by coupling a core oscillator to a precipitation and a complexation reaction. We again choose the BrO_3^-–SO_3^{2-}–$Fe(CN)_6^{4-}$ reaction as the core reaction O.

If we take the precipitation reaction as equation (2) and add F^- ion, the reaction

$$Al^{3+} + 4F^- \leftrightarrow AlF_4^- \quad \beta_4 = [AlF_4^-]/[Al^{3+}][F^-]^4 = 5 \times 10^{17} \quad (3)$$

with cumulative formation constant β_4 for the complex ion AlF_4^-, serves as a second equilibrium coupled to equation (2). As reaction O oscillates, at low pH, Al^{3+} is released in equation (2), causing complexation with F^- and a resulting drop in the free $[F^-]$. When the pH rises, the equilibrium in equation (2) shifts back to the formation of $Al(OH)_3$, and part of the complexed fluoride is released. Fluoride ion pulses measured with a fluoride-ISE in the BrO_3^-–SO_3^{2-}–$Fe(CN)_6^{4-}$ + $Al(NO_3)_3$ + NaF system are seen in Fig. 5. We note that the fluoride-ISE responds to the change of pH (below pH 5) and $[Al^{3+}]$ in the absence of fluoride ions, but the potential of the electrode measured at any pH and $[Al^{3+}]$ falls far above the range of potentials recorded when fluoride ions are also present at a concentration of 10^{-5}–10^{-2} M, that is, the full line in Fig. 5 indicates the changes in $[F^-]$.

In the examples given here, we have used as the 'core' reaction O a pH oscillator that encompasses the pH range 3–6. Other pH oscillators are available in different pH ranges[11], which allows us to use for reaction E complexation reactions with different stability constants or with different ligands (for example, amino acids), and precipitation reactions with different solubility products, though one must take care to ensure that the components of reaction E do not interfere with the oscillatory functioning of reaction O. It is possible, of course, to utilize oscillators that produce periodic variations in species other than H^+ and to seek equilibrium reactions to couple to those species. Bromide and iodide ions may be particularly promising in this regard.

If oscillators of this type can be built from biocompatible components, then it should be possible to use them as probes of the response of biological oscillators to periodic concentration perturbations. For example, interfacing an inorganic oscillator like the Ca^{2+} system described here to one of the many biological systems that generate oscillations in the concentration of that ion[12] would make it possible to investigate the effects of reciprocal feedback from the living to the nonliving system. Similarly, oscillators involving Na^+, K^+, or Ca^{2+} could be linked by an artificial synapse[13] to a neuron to probe its response to perturbations. In an unstirred reactor, one could create spatial patterns of a chosen species and study their interactions with natural pattern-forming systems. It is also interesting to speculate whether some kinds of oscillatory behaviour in living systems could be produced by a similar scheme of coupling to a core oscillator in order to generate periodic behaviour in chemical species whose concentration levels would not otherwise oscillate. □

Received 15 October; accepted 22 November 2004; doi:10.1038/nature03214.

1. Bray, W. C. A periodic reaction in homogeneous solution and its relation to catalysis. *J. Am. Chem. Soc.* **43,** 1262–1267 (1921).
2. Belousov, B. P. A periodic reaction and its mechanism. In *Sbornik Referatov po Radiatsionni Meditsine* 145 (Medgiz, Moscow, 1958).
3. Zhabotinsky, A. M. Periodic kinetics of oxidation of malonic acid in solution. *Biofizika* **9,** 306–311 (1964).
4. Epstein, I. R., Kustin, K., De Kepper, P. & Orbán, M. Oscillating chemical reactions. *Sci. Am.* **248,** 112–123 (1983).
5. De Kepper, P., Kustin, K. & Epstein, I. R. A systematically designed homogeneous oscillating reaction: the arsenite–iodate–chlorite system. *J. Am. Chem. Soc.* **103,** 2133–2134 (1981).
6. Sagués, F. & Epstein, I. R. Nonlinear chemical dynamics. *Dalton Trans.*, 1201–1217 (2003).
7. Orbán, M., De Kepper, P. & Epstein, I. R. Minimal bromate oscillator: Bromate–bromide–catalyst. *J. Am. Chem. Soc.* **104,** 2657–2658 (1982).

8. Richter, P. H. & Ross, J. Concentration oscillations and efficiency: Glycolysis. *Science* **211,** 715–717 (1981).
9. Harris, D. C. *Quantitative Chemical Analysis* 5th edn 312–313 (Freeman, New York, 1999).
10. Edblom, E. C., Luo, Y., Orbán, M., Kustin, K. & Epstein, I. R. Kinetics and mechanism of the oscillatory bromate–sulfite–ferrocyanide reaction. *J. Phys. Chem.* **93,** 2722–2727 (1989).
11. Rábai, G., Orbán, M. & Epstein, I. R. Design of pH-regulated oscillators. *Acc. Chem. Res.* **23,** 258–263 (1990).
12. Berridge, M. J. Calcium oscillators. *J. Biol. Chem.* **265,** 9583–9586 (1990).
13. Szucs, A. *et al.* Interacting biological and electronic neurons generate realistic oscillatory rhythms. *Neuroreport* **11,** 563–569 (2000).

Acknowledgements This work was supported by the Hungarian Academy of Sciences (HAS), the US National Science Foundation (NSF) and a US-Hungarian Cooperative Research Grant from NSF and HAS. We thank L. Yang for assistance in preparing the figures.

Competing interests statement The authors declare that they have no competing financial interests.

Correspondence and requests for materials should be addressed to I.R.E. (epstein@brandeis.edu).

Efficient export of carbon to the deep ocean through dissolved organic matter

Charles S. Hopkinson Jr & Joseph J. Vallino

The Ecosystems Center, Marine Biological Laboratory, Woods Hole, Massachusetts 02543, USA

Oceanic dissolved organic carbon (DOC) constitutes one of the largest pools of reduced carbon in the biosphere. Estimated DOC export from the surface ocean represents 20% of total organic carbon flux to the deep ocean[1–3], which constitutes a primary control on atmospheric carbon dioxide levels[4]. DOC is the carbon component of dissolved organic matter (DOM) and an accurate quantification of DOM pools, fluxes and their controls is therefore critical to understanding oceanic carbon cycling. DOC export is directly coupled with dissolved organic nitrogen and phosphorus export. However, the C:N:P stoichiometry (by atoms) of DOM dynamics is poorly understood. Here we study the stoichiometry of the DOM pool and of DOM decomposition in continental shelf, continental slope and central ocean gyre environments. We find that DOM is remineralized and produced with a C:N:P stoichiometry of 199:20:1 that is substantially lower than for bulk pools (typically >775:54:1), but greater than for particulate organic matter (106:16:1—the Redfield ratio). Thus for a given mass of new N and P introduced into surface water, more DOC can be exported than would occur at the Redfield ratio. This may contribute to the excess respiration estimated to occur in the interior ocean[5]. Our results place an explicit constraint on global carbon export and elemental balance via advective pathways.

Accurate quantification of DOM pools, fluxes and their controls is critical to understanding oceanic carbon cycling and how the oceans will respond to increasing concentrations of atmospheric CO_2 and climate change[4,6,7]. The nitrogen and phosphorus cycles in the ocean are closely coupled with the carbon cycle and the Redfield ratio has been a unifying paradigm describing the stoichiometry of this coupling. It is an implicit assumption that the amount of carbon that can be exported to depth is directly related to the quantity of 'new' nutrients (NO_3^- and PO_4^{3-}) that are brought back to the surface through physical processes and added via nitrogen fixation and atmospheric deposition[8]. The production, export and remineralization of particulate organic matter, which accounts for 80% of total organic carbon flux to the deep ocean, operate with Redfield stoichiometry. An extreme paucity of data on simultaneous measures of DOC, dissolved organic nitrogen and phosphorus (DON and DOP) and lack of information on production, decomposition and export processes have held back progress in understanding the coupled dynamics of these pools. Recent studies of DOM dynamics show large departures from Redfield trajectories. DOM pools in surface and deep-ocean waters deviate widely from the Redfield ratio with reports of C:N:P ratios in excess of 4,000:300:1 (refs 9–12). Production of new DOM is often N-poor relative to C, with elevated C:N ratios measured during and immediately after diatom blooms[13]. A number of studies have shown that N and P preferentially remineralize relative to C (refs 9–11 and 14–16). But how can overall organic matter export conform to the Redfield ratio while DOM stoichiometry apparently deviates so greatly? Is our understanding of the magnitude of C export relative to N and P correct? If estimates of DOC export are correct and the stoichiometry of DOM export deviates substantially from the Redfield ratio, we urgently need to understand the mechanisms that control the stoichiometry of DOM production, export and remineralization so that predictions of the response to climate and CO_2 changes can be made.

We studied DOM pool and decomposition stoichiometry in continental-shelf, continental-slope and central-ocean-gyre environments. The observed C:N:P ratios for bulk DOM deviated substantially from the Redfield ratio. The average C:N:P ratio for all samples across all depths was 778:54:1. In general, C:N:P ratios were lower when DOM concentrations were higher and were higher with low DOM concentrations (Table 1). The average C:N, C:P and N:P ratios for surface waters with increased DOM concentrations were 14:1, 374:1 and 27:1, respectively, and these ratios differed only moderately between locations and time (Table 1). The average C:N, C:P and N:P ratios for deep waters, which have low DOM concentrations, were substantially higher, averaging 22:1, 3511:1 and 202:1, respectively.

The stoichiometry of production and decomposition is determined from the slope of DOM element–element plots for samples collected throughout the ocean, for example, DON versus DOC (Fig. 1). It is implicit in this type of analysis that the stoichiometry of production and decomposition is the same. The stoichiometry of the decomposable DOM pool averaged 199:20:1. Thus C:N and C:P ratios were significantly C-rich: 62% and 87% higher than the Redfield ratio. The N:P ratio was higher than the Redfield, but not significantly (20 versus 16:1). These results show that the C:N:P stoichiometry of DOM decomposition is much lower than the C:N:P ratios of surface or deep-water pools. Although the bulk DOM is extremely rich in C relative to N and N relative to P, the space-for-time patterns of DOM decomposition indicate that the stoichiometry of the degradable DOM pool is also C-rich but at a level intermediate to that of Redfield and bulk DOM.

The decomposition stoichiometry was also determined independently by directly observing changes in DOM composition during laboratory incubations of shelf and slope waters. The incubations revealed (Fig. 2) that the decomposable fraction of the bulk DOM varied for DOC, DON and DOP, but loss rates were similar[11]. The stoichiometry of the fraction that decomposed was substantially lower than that of the initial bulk pool and averaged 221:20:1. Laboratory decomposition studies agreed favourably with the field space-for-time approach, suggesting that the patterns found from field observations are robust.

Although there are numerous reports of greatly increased C:N ratios of DOM production, especially after phytoplankton blooms (see, for example, ref. 13), our results indicate that, on average, the stoichiometry is only moderately increased (10.7:1). The C:N:P of upwelled, deep-water DOM (3511:202:1) is brought closer to the Redfield ratio (C:N:P drops) in surface waters as new DOM is